Flow by a Porous Shrinking Surface in a Rotating Frame

Tasawar Hayat[a], Sania Iram[a], Tariq Javed[b], and Saleem Asghar[c]

[a] Department of Mathematics, Quaid-I-Azam University 45320, Islamabad 44000, Pakistan
[b] Faculty of Basic and Applied Sciences, International Islamic University, Islamabad 44000, Pakistan
[c] Department of Mathematics, Comsats Institute of Information Technology Islamabad 44000, Pakistan

Reprint requests to T. H.; Fax: +92 51 2601171. E-mail: pensy_t@yahoo.com

We derive series solution of a nonlinear problem which models the magnetohydrodynamic (MHD) shrinking flow due to a porous plate in a rotating frame of reference. The governing partial differential equations are first converted into ordinary differential equations and then solved by homotopy analysis method. The convergence of the derived series solution is carefully analyzed. Graphical results are presented to examine the role of various interesting parameters.

Key words: Rotating Frame; Homotopy Analysis Solution; Shrinking Flow.

1. Introduction

In view of engineering and industrial applications, the boundary layer flows have received substantial attention in the past. Some of the typical applications of such flows include polymer sheet extrusion from a dye, glass fiber and paper production, drawing of plastic films, and many others. In 1961, Sakiadis [1] made the first study of boundary layer flow over a continuous solid surface with constant speed. An extensive literature is now available on the two-dimensional boundary layer flow bounded by a stretching surface when the stretching velocity is linearly proportional to the distance from a fixed origin. Recent investigations in this direction can be seen through the studies [2 – 10]. Some studies [11 – 14] dealing with the flow induced by a nonlinear stretching velocity are also available.

Very little attention is given to the three-dimensional shrinking flow in a rotating frame of reference. Such flow analysis is not available when the suction is imposed on the lower plate (shrinking surface) whereas the upper plate exhibits injection. An incompressible viscous fluid fills the space between the two porous plates. Moreover the fluid is electrically conducting and the plates are non-conducting. Note that the electrically conducting fluids such as nuclear fuel slurries, liquid metals, mercury amalgams, biological fluids, lubrication of oils and certain greases have promising applications in the absence as well as in the presence of a magnetic field. In addition, the flows in a rotating frame have many applications in geophysics and astro-physics. In view of these facts the present communication is organized as follows.

Section 2 describes the formulation of the problem. Analytic solutions of arising nonlinear differential equations are constructed by invoking a recently developed technique by Liao [15, 16], namely the homotopy analysis method (HAM) in Section 3. Since the analytic solutions of nonlinear differential equations are one of the central tenets of perpetual interest in mathematical physics, the HAM has been successfully applied in the past for various problems [17 – 30]. Section 4 consists of the convergence analysis. Results and discussion are presented in Section 5. Section 6 comprises final remarks.

2. Problem Formulation

Here we consider the steady, three-dimensional flow of an incompressible viscous fluid bounded by two horizontal porous plates at $y = \pm h$. The whole system (fluid and plates) is in a rotating frame with a constant angular velocity Ω along the y-axis. The flow between the two plates is engendered by a shrinking surface at $y = -h$. Furthermore, the fluid is electrically conducting by a constant magnetic field $\mathbf{B}_0$ applied in y-direction. The physical model of the present flow situation is shown in Figure 1.

The mathematical statement of the considered problem is [18]:

$$\frac{\partial u}{\partial x} + \frac{\partial v}{\partial y} = 0, \tag{1}$$
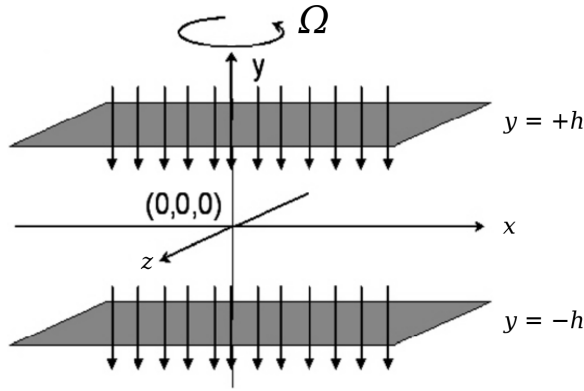
Fig. 1. Physical configuration for flow.

$$u\frac{\partial u}{\partial x} + v\frac{\partial u}{\partial y} + 2\Omega w$$
$$= -\frac{1}{\rho}\frac{\partial p^*}{\partial x} + v\left[\frac{\partial^2 u}{\partial x^2} + \frac{\partial^2 u}{\partial y^2}\right] - \frac{\sigma B_0^2 u}{\rho}, \quad (2)$$

$$v\frac{\partial v}{\partial y} = -\frac{1}{\rho}\frac{\partial p^*}{\partial y} + v\frac{\partial^2 v}{\partial y^2}, \quad (3)$$

$$u\frac{\partial w}{\partial x} + v\frac{\partial w}{\partial y} - 2\Omega u = v\left[\frac{\partial^2 w}{\partial x^2} + \frac{\partial^2 w}{\partial y^2}\right] - \frac{\sigma B_0^2 w}{\rho}, \quad (4)$$

$$u = -ax, \quad v = -V, \quad w = 0, \quad \text{at } y = -h,$$
$$u = 0, \quad v = V, \quad w = 0, \quad \text{at } y = h. \quad (5)$$

In the above equations u, v, and w are the velocity components in x-, y-, and z-directions, respectively, ρ is the density, v the kinematic viscosity, σ the electrical conductivity, ρ^* the modified pressure, $a > 0$ the shrinking constant, $V > 0$ the suction velocity, and $V < 0$ the injection velocity.

Writing [18]

$$\eta = \frac{y}{h}, \quad u = -axf'(\eta),$$
$$v = ahf(\eta), \quad w = axg(\eta), \quad (6)$$

(1) is satisfied, and (2)−(5), after using above similarity transformations, become

$$f'''' - M^2 f'' + 2K^2 g' + R(f'f'' - ff''') = 0, \quad (7)$$

$$g'' - M^2 g - 2K^2 f' + R(f'g - fg') = 0, \quad (8)$$

$$f = -\lambda, \quad f' = 1, \quad g = 0, \quad \text{at } \eta = -1,$$
$$f = \lambda, \quad f' = 0, \quad g = 0, \quad \text{at } \eta = 1, \quad (9)$$

where the prime indicates the differentiation with respect to η and the suction parameter λ, the viscosity parameter R, the Hartman number M, and the rotation parameter K are defined by

$$\lambda = \frac{v}{ah}, \quad R = \frac{ah^2}{v}, \quad M^2 = \frac{\sigma B_0^2 h^2}{\rho v}, \quad K^2 = \frac{\Omega h^2}{v}.$$

In the next section we shall demonstrate the solution of (7)−(9) by the means of the homotopy analysis method.

3. Solutions by Homotopy Analysis Method (HAM)

The series solutions of f and g are expressed as

$$f(\eta) = \sum_{m=0}^{\infty} a_m \eta^m, \quad g(\eta) = \sum_{m=0}^{\infty} b_m \eta^m, \quad (10)$$

where a_m and b_m ($m = 1, 2, \ldots$) are the coefficients to be determined.

By the 'rule of solution expression' (10) and the boundary conditions (9), the initial approximations f_0, g_0, and the auxiliary linear operators $\mathcal{L}_i$ ($i = 1, 2$) are chosen as

$$f_0(\eta) = \frac{1}{4} + \frac{(-1 + 6\lambda)}{4}\eta - \frac{\eta^2}{4} + \frac{(1 + 2\lambda)}{4}\eta^3, \quad (11)$$

$$g_0(\eta) = 0, \quad (12)$$

$$\mathcal{L}_1(f) = \frac{d^4 f}{d\eta^4}, \quad (13)$$

$$\mathcal{L}_2(g) = \frac{d^2 g}{d\eta^2}. \quad (14)$$

Obviously, the operators $\mathcal{L}_i$ ($i = 1, 2$) satisfy the following properties:

$$\mathcal{L}_1[C_1\eta^3 + C_2\eta^2 + C_3\eta + C_4] = 0, \quad (15)$$

$$\mathcal{L}_2[C_5\eta + C_6] = 0, \quad (16)$$

where C_i ($i = 1−6$) are the constants.

The 'zeroth-order deformation problems' are constructed as follows:

$$(1-p)\mathcal{L}_1[\hat{f}(\eta;p) - f_0(\eta)] = p\hbar\mathcal{N}_1[\hat{f}(\eta;p), \hat{g}(\eta;p)], \quad (17)$$

$$\mathcal{N}_1[\hat{f}(\eta;p),\hat{g}(\eta;p)] = \frac{\partial^4 \hat{f}(\eta;p)}{\partial\eta^4} - M^2\frac{\partial^2 \hat{f}(\eta;p)}{\partial\eta^2}$$

$$+ 2K^2\frac{\partial\hat{g}(\eta;p)}{\partial\eta} + R\left(\frac{\partial\hat{f}(\eta;p)}{\partial\eta}\frac{\partial^2\hat{f}(\eta;p)}{\partial\eta^2}\right. \tag{18}$$

$$\left. -\hat{f}(\eta;p)\frac{\partial^3\hat{f}(\eta;p)}{\partial\eta^3}\right),$$

$$\hat{f}(-1;p) = -\lambda, \quad \hat{f}'(-1;p) = 1,$$
$$\hat{f}(1;p) = \lambda, \quad \hat{f}'(1;p) = 0, \tag{19}$$

$$(1-p)\mathcal{L}_2[\hat{g}(\eta;p) - g_0(\eta)] = p\hbar\mathcal{N}_2[\hat{g}(\eta;p),\hat{f}(\eta;p)], \tag{20}$$

$$\mathcal{N}_2[\hat{g}f(\eta;p),\hat{f}(\eta;p)] = \frac{\partial^2\hat{g}(\eta;p)}{\partial\eta^2} - M^2\hat{g}(\eta;p)$$

$$-2K^2\frac{\partial\hat{f}(\eta;p)}{\partial\eta} + R\left(\frac{\partial\hat{f}(\eta;p)}{\partial\eta}\hat{g}(\eta;p)\right. \tag{21}$$

$$\left. -\hat{f}(\eta;p)\frac{\partial\hat{g}(\eta;p)}{\partial\eta}\right),$$

$$\hat{g}(-1;p) = 0, \quad \hat{g}(1;p) = 0, \tag{22}$$

in which $\hbar$ is the auxiliary non-zero parameter and $p \in [0,1]$ is an embedding parameter. When the parameter p increases from 0 to 1, the solution $\hat{f}(\eta;p)$ varies from $f_0(\eta)$ to $f(\eta)$ and $\hat{g}(\eta;p)$ from $g_0(\eta)$ to $g(\eta)$. Expanding $\hat{f}(\eta;p)$ and $\hat{g}(\eta,p)$ in Taylor series and considering that the resulting series are convergent at $p = 1$ one obtains

$$f(\eta) = f_0(\eta) + \sum_{m=1}^{\infty} f_m(\eta),$$
$$g(\eta) = g_0(\eta) + \sum_{m=1}^{\infty} g_m(\eta), \tag{23}$$

$$f_m(\eta) = \frac{1}{m!}\frac{\partial^m\hat{f}(\eta;p)}{\partial p^m}\bigg|_{p=0},$$
$$g_m(\eta) = \frac{1}{m!}\frac{\partial^m\hat{g}(\eta;p)}{\partial p^m}\bigg|_{p=0}. \tag{24}$$

Differentiating 'zeroth-order deformation equations' m times with respect to p, setting $p = 0$, and finally dividing them by $m!$, one has the following 'mth-order deformation' problems

$$\mathcal{L}_1[f_m(\eta) - \chi_m f_{m-1}(\eta)] = \hbar\mathcal{R}_{1m}(\eta), \tag{25}$$

$$\mathcal{L}_2[g_m(\eta) - \chi_m g_{m-1}(\eta)] = \hbar\mathcal{R}_{2m}(\eta), \tag{26}$$

$$f_m(-1) = f'_m(-1) = f_m(1) = f'_m(1) = 0, \tag{27}$$

$$g_m(-1) = g_m(1) = 0, \tag{28}$$

$$\mathcal{R}_{1m}(\eta) = f'''_{m-1} - M^2 f''_{m-1} + 2K^2 g'_{m-1}$$
$$+ R\sum_{k=0}^{m=-1}[f'_{m-1-k}f''_k - f_{m-1-k}f'''_k], \tag{29}$$

$$\mathcal{R}_{2m}(\eta) = g''_{m-1} - M^2 g_{m-1} - 2K^2 f'_{m-1}$$
$$+ R\sum_{k=0}^{m=-1}[g_{m-1-k}f'_k - g'_{m-1-k}f_k], \tag{30}$$

$$\chi_m = \begin{cases} 0, m \leq 1, \\ 1, m > 1. \end{cases} \tag{31}$$

By Mathematica, the mth-order approximations of f and g are given by

$$f(\eta) \approx F_m(\eta) = \sum_{m=0}^{\infty} f_m(\eta)$$
$$= \lim_{M\to\infty}\left[\sum_{n=1}^{4M+3}\left(\sum_{m=n-1}^{4M+2} a_{m,n}\eta^n\right)\right], \tag{32}$$

$$g(\eta) \approx G_m(\eta) = \sum_{m=0}^{\infty} g_m(\eta)$$
$$= \lim_{M\to\infty}\left[\sum_{n=1}^{4M+2}\left(\sum_{m=n-1}^{4M+1} b_{m,n}\eta^n\right)\right], \tag{33}$$

where $a_{m,n}$ and $b_{m,n}$ are constants of $f(\eta)$ and $g(\eta)$, respectively.

4. Convergence of HAM Solutions

As pointed out by Liao [15], the homotopy analysis method (HAM) provides us with a family of solution expressions in the auxiliary parameter $\hbar$. As a result, the convergence and rate of solution series are dependent upon the auxiliary parameter $\hbar$ and thus can be greatly enlarged by means of choosing a proper value for $\hbar$. This provides us with a convenient way to adjust and control convergence region and rate of solution series given by HAM. In general, by means of the so-called $\hbar$-curve, it is straightforward to choose an appropriate range for $\hbar$ which ensures the convergence of the solution series.

To ensure the convergence of the series solutions (29) and (30), we draw $\hbar$-curves to find the reasonable values of $\hbar$. Figure 2 shows the $\hbar$-curves of $f''(0)$ and $g'(0)$ for 20th-order of approximation.
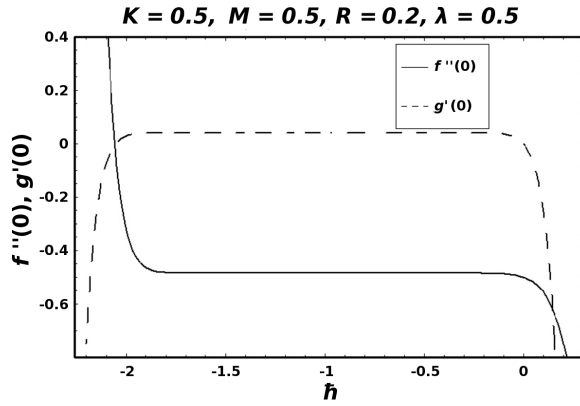
Fig. 2. $\hbar$-curves for the 20th-order of approximation.
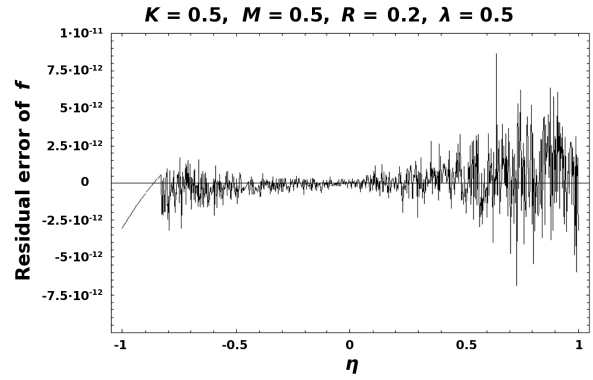
Fig. 5. Residual error of f when $\hbar = -1.0$ at the 15th-order of approximation.
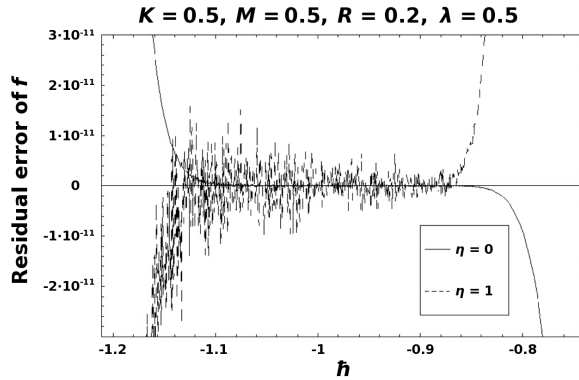
Fig. 3. Residual error of the 15th-order of solution for f.
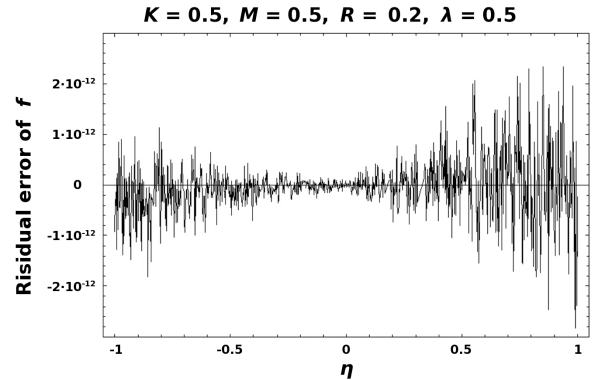
Fig. 6. Residual error of f when $\hbar = -0.9$ at the 15th-order of approximation.
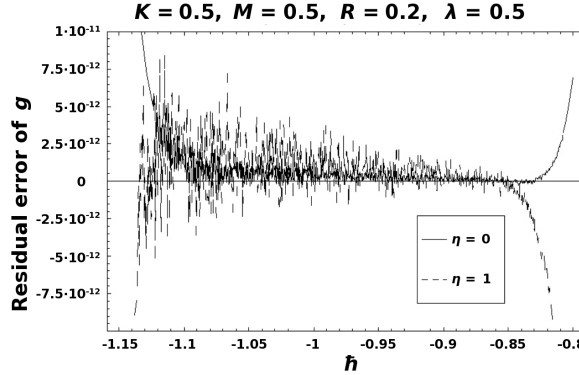
Fig. 4. Residual error of the 15th-order of solution for g.

Fig. 7. Residual error of g when $\hbar = -1.0$ at the 15th-order of approximation.

This figure indicates that the region for the admissible values of $\hbar$ is $-1.8 \leq \hbar \leq -0.1$.

We can investigate the influence of $\hbar$ on the residual errors defined as:

Residual error of $f \approx F_m'''' - M^2 F_m'' + 2K^2 G_m' + R(F_m' F_m'' - F_m F_m''')$.
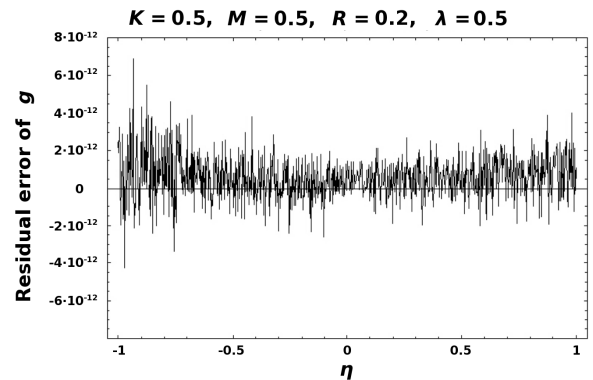
Residual error of $g \approx G_m'' - M^2 G_m - 2K^2 F_m' + R(F_m' G_m - F_m G_m')$.

Figures 3 and 4 depict the residual errors of the 15th-order of solution for f and g at $\eta = 0$ and $\eta = 1$. These
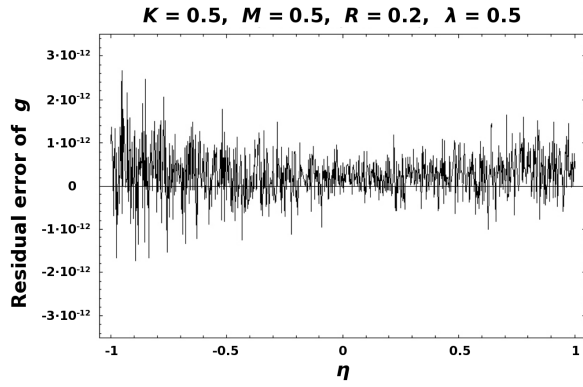
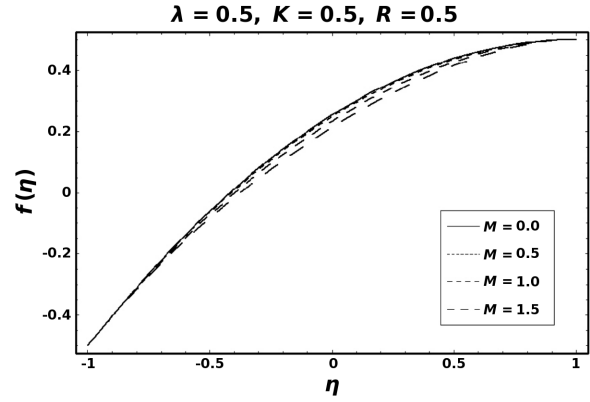Fig. 8. Residual error of g when $\hbar = -0.9$ at the 15th-order of approximation.

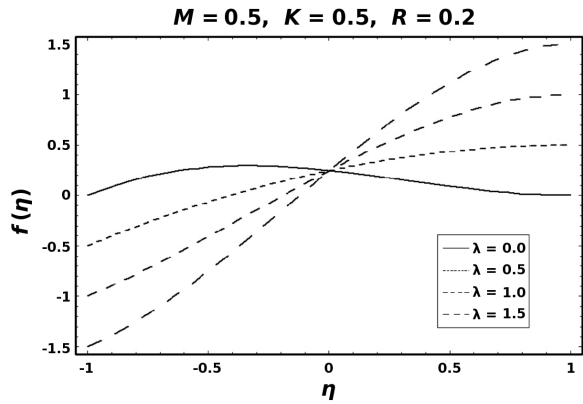Fig. 9. Influence of λ on f when $\hbar = -0.9$.

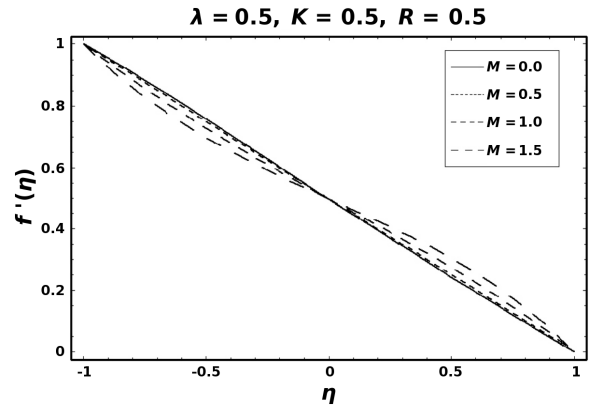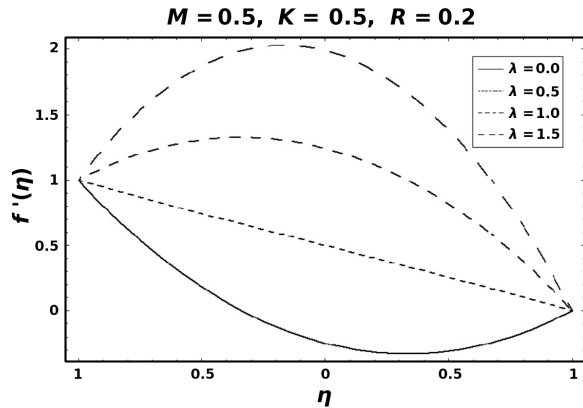Fig. 10. Influence of λ on f' when $\hbar = -0.9$.

Fig. 11. Influence of M on f when $\hbar = -0.9$.

Fig. 12. Influence of M on f' when $\hbar = -0.9$.
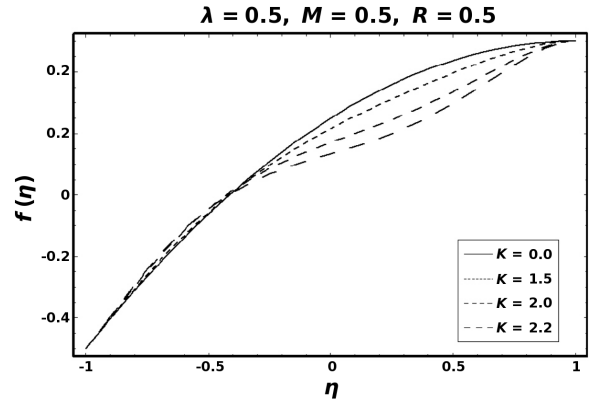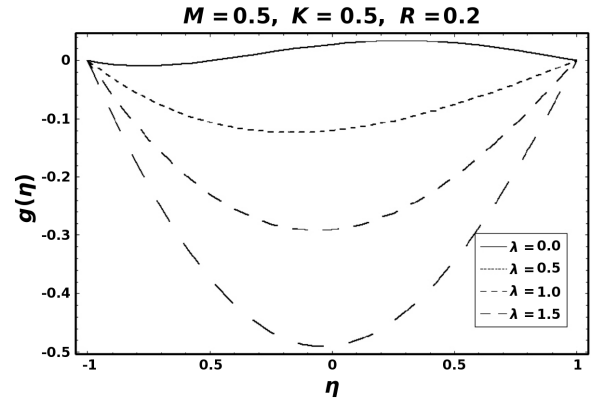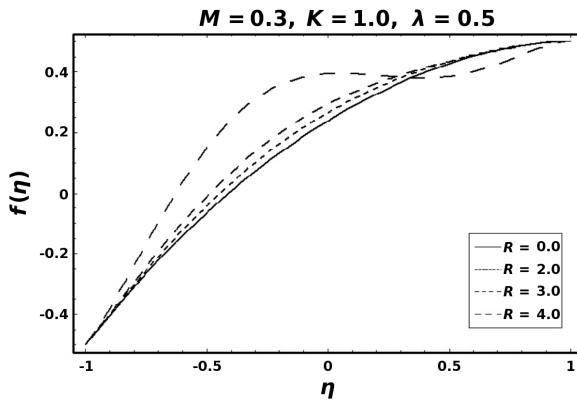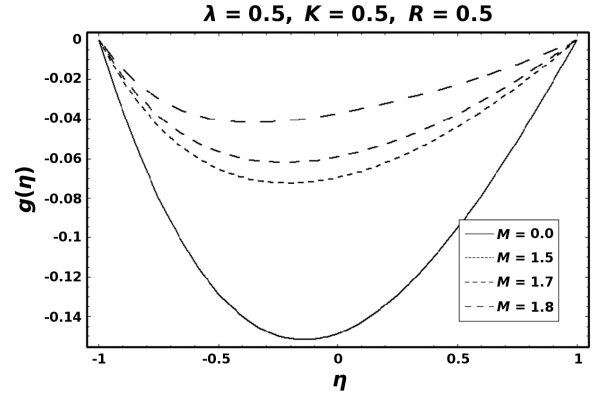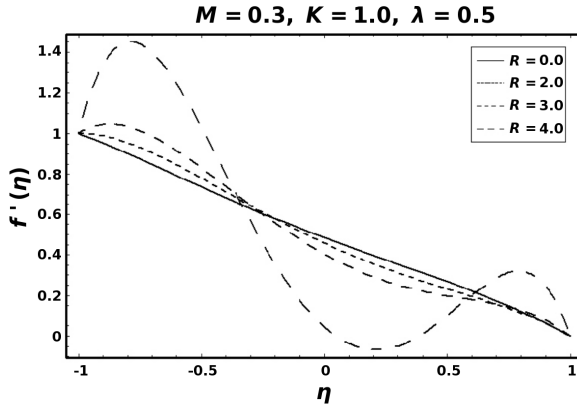

Fig. 13. Influence of K on f when $\hbar = -0.9$.

figures indicate that the range for values of $\hbar$ giving approximately zero residual error is $-1.1 \le \hbar \le -0.88$.

Figures 5 and 6 give the residual error of f for the whole region of η at $\hbar = -1.0$ and -0.9, respectively.

Similarly, Figures 7 and 8 describe the residual error of g for the whole region of η at $\hbar = -1.0$ and -0.9, respectively. It is found from these figures that for these values of parameters the best value of $\hbar$ for the whole region of η is -0.9.
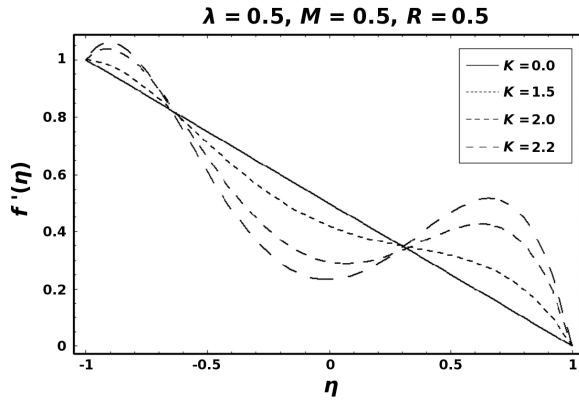
Fig. 14. Influence of K on f' when $\hbar = -0.9$.

Fig. 15. Influence of R on f when $\hbar = -0.9$.

Fig. 16. Influence of R on f' when $\hbar = -0.9$.

Similarly, by drawing the $\hbar$-curves and residual error curves, we can choose the best value of $\hbar$ for the rest of the values of the parameters.

Fig. 17. Influence of λ on g when $\hbar = -0.9$.

Fig. 18. Influence of M on g when $\hbar = -0.9$.
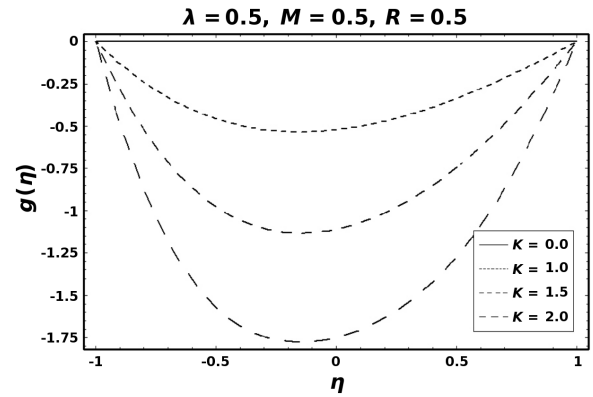
Fig. 19. Influence of K on g when $\hbar = -0.9$.

5. Results and Discussion

This section deals with the variations of some sundry parameters on f, f', and g. Therefore,
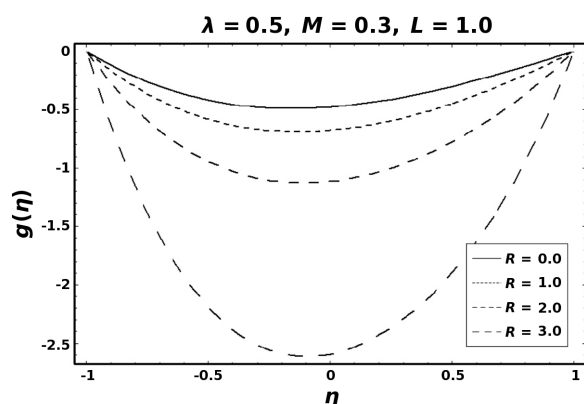
λ = 0.5, M = 0.3, L = 1.0

Fig. 20. Influence of R on g when $\hbar = -0.9$.

Figures 9–20 have been sketched in order to see such variations. Particularly, the variations of λ, M, K, and R in these figures are displayed. The variation of λ on f and f' is shown in Figures 9 and 10, respectively. It is revealed that f decreases (increases) in the lower (upper) half of channel when λ is increased. Also f' increases by increasing λ (Fig. 10).

The effects of M on f and f' are analyzed in Figures 11 and 12. Clearly f is a decreasing function of M. However f' decreases (increases) in the lower (upper) half of the channel when M increases. Such observation is expected because the effect of magnetic force is against the flow direction. The role of K on f and f' can be seen in Figures 13 and 14. Here f increases near the lower plate (shrinking surface) and decreases by increasing K. The layer thickness near the lower plate decreases. This corresponds to the thinning property of the rotation. It is noticed that f' increases near the plates by increasing K and decreases at the centre of channel (Fig. 14).

Figures 15 and 16 have been prepared in order to examine the effects of R on f and f'. Figure 15 shows that in the lower half of channel f increases when R increases. However, the variation of f in the upper half channel is opposite. The variations of f' in Figure 16 are similar to that of Figure 14 in a qualitative sense. Such variations are larger in case of viscosity parameter R.

Figures 17–20 illustrate the effects of λ, M, K, and R on g. Here g decreases by increasing λ (Fig. 17). It is also noted that such decrease is larger at the centre of channel when compared at the plates. Through Figure 18 one can easily see that g is an increasing function of M. Figures 17 and 19 indicate that the role of λ and K on g are similar. It is noticed from Figure 20 that g has similar variation for large R when compared with K. However the change is slightly larger in the case of R.

6. Final Remarks

This study discusses the three-dimensional rotating flow between two porous plates. The upper plate subjects the injection and the lower one has the suction. The relevant formulation is carefully made and the arising nonlinear problem is solved analytically by a powerful tool, namely the homotopy analysis method. From the presented analysis the following observations may be drawn:

• The variations of R on f in lower and upper parts of the channel are different.
• Effects of K and R on f' are qualitatively similar.
• The influences of λ and K on g are qualitatively similar.
• An increase in M reduces f.

[1] B. C. Sakiadis, AIChE J. **7**, 26 (1961).
[2] S. J. Liao, Commun. Nonlinear Sci. Numer. Simul. **11**, 326 (2006).
[3] R. Cortell, Phys. Lett. A **357**, 298 (2006).
[4] T. Hayat, Z. Abbas, and M. Sajid, Phys. Lett. A **358**, 396 (2006).
[5] R. Cortell, Int. J. Nonlinear Mech. **41**, 78 (2006).
[6] P. D. Ariel, T. Hayat, and S. Asghar, Acta Mech. **187**, 29 (2006).
[7] R. Cortell, Appl. Math. Comput. **168**, 557 (2005).
[8] Z. Abbas, T. Hayat, M. Sajid, and S. Asghar, Math. Comput. Model. **48**, 518 (2008).
[9] K. Vajravelu and T. Roper, Int. J. Nonlinear Mech. **34**, 1031 (1999).
[10] I. C. Liu, Int. J. Nonlinear Mech. **40**, 465 (2005).
[11] T. Hayat, Z. Abbas, and T. Javed, Phys. Lett. A **372**, 637 (2008).
[12] M. Sajid, T. Hayat, S. Asghar, and K. Vajravelu, Arch. Appl. Mech. **78**, 127 (2008).
[13] K. Vajravelu, Appl. Math. Comput. **124**, 281 (2001).
[14] R. Cortell, Phys. Lett. A **372**, 631 (2008).
[15] S. J. Liao, Beyond perturbation: Introduction to homotopy analysis method, Chapman and Hall, CRC Press, Boca Raton (2003).
[16] S. J. Liao, Int. J. Heat and Mass Transfer **48**, 2529 (2005).
[17] T. Hayat and M. Sajid, Int. J. Heat and Mass Transfer **50**, 75 (2007).

[18] T. Hayat, Z. Abbas, T. Javed, and M. Sajid, Chaos, Solitons, and Fractals **39**, 1615 (2009).

[19] M. Sajid, T. Hayat, and I. Pop, Nonlinear Anal.: Real Word Application **9**, 1811 (2008).

[20] T. Hayat and Z. Abbas, Chaos, Solitons, and Fractals **38**, 556 (2008).

[21] M. Sajid and T. Hayat, Chaos, Solitons, and Fractals **38**, 506 (2008).

[22] S. J. Liao, Commun. Nonlinear Sci. Numer. Simul. **11**, 326 (2006).

[23] C. Yang and S. J. Liao, Commun. Nonlinear Sci. Numer. Simul. **11**, 83 (2006).

[24] W. Wu and S. J. Liao, Chaos, Solitons, and Fractals **26**, 177 (2005).

[25] S. P. Zhu, Quan. Finance **6**, 229 (2006).

[26] S. Abbasbandy, Chem. Eng. J. **136**, 144 (2008).

[27] S. Abbasbandy and F. S. Zakaria, Nonlinear Dyn. **51**, 83 (2008).

[28] S. Abbasbandy, ZAMP **59**, 51 (2008).

[29] F. M. Allan, Appl. Maths. Comput. **190**, 6 (2007).

[30] M. Sajid, T. Javed, and T. Hayat, Nonlinear Dyn. **51**, 259 (2008).